Hydrodynamic and Biological Assessment of Modified Meander C-type Fishway to pass Rainbow Trout (Oncorhynchus mykiss) Fish Species

1- Saman Baharvand

Department of Civil Engineering, Jundi-Shapur University of Technology, Dezful, Iran.

Email : Saman.baharvand@mavs.uta.edu

ORCID : 0000-0002-1184-3391

2- Babak Lashkar-Ara*

Associate Professor **(Corresponding Author)**

Department of Civil Engineering, Jundi-Shapur University of Technology, Dezful, Iran.

Email*: Lashkarara@jsu.ac.ir

Phone :

ORCID : 0000-0001-7112-2548

Abstract

Human-made structures are the main obstacles constructed on the river's cross-section, preventing fishes from swimming toward the ideal spawning zones upstream of the streams. Present study determines the hydrodynamic performance of a Modified Meander C-type Fishway (MMCF) with a 20% bed slope using both physical and numerical modeling. Specifically, the study investigates the variations in Turbulent Kinetic Energy (TKE) and fluid friction coefficient (C_f) in the pools, which are critical hydraulic characteristics of the fishway. The study examines the TKE variation for different discharge and geometry scenarios through the longest path in the pools of the MMCF. This analysis was performed at an average depth of 0.5d to investigate the possibility of creating resting pool areas in the fishway, where fish can rest during their migration. In addition, the propulsive energy of three hypothetical rainbow trout fish

species was estimated based on their physical characteristics, including weight, length, swimming speed, and time to exhaustion, using empirical relationships. The propulsive energy of the fish species was evaluated for different levels of volumetric energy dissipation in the measuring pool of fishway, and the study discussed the ability of migratory fish species to safely navigate through the pools of fishway.

Keywords: Meander Fishway, Experimental Modeling, Computational Fluid Dynamics, Turbulence, Aquatic Suitability Index

1 Introduction

Fish passage structures, also known as fishways, are constructed to aid the migration of fish species through obstacles in rivers. These structures can be classified into several types including pool and weir, Vertical Slot Fishway (VSF), culvert, Denil fishways, and nature-based passages (Clay) [1], (Weibel and Peter) [2], (Katopodis and Williams) [3]. The main objective of these structures is to modify the surrounding environment to establish optimal habitat conditions that are suitable for aquatic species (Baki et al.) [4], (Katopodis et al.) [5], (Rajaratnam et al.) [6]. To achieve this goal, researchers such as Rajaratnam and Katopodis [7], Marriner et al. [8], and Decker [9] have conducted extensive studies on the geometry and flow pattern structure of various fishway types. Additionally, Noonan et al. [10], and Bunt et al. [11] have investigated several hydraulic and biological factors to improve the efficiency of fish passage structures.

Physical modeling, numerical analysis, and field studies have shown that the Vertical Slot Fishway (VSF) is a robust design that enables various fish species with different swimming abilities to migrate upstream (DVWK) [12], (Puertas et al.) [13], (Marriner et al.) [8], (Quaranta et al.) [14]. According to Baki and Azimi [15], the crucial aspect of the

VSF is its ability to function under a range of upstream and downstream river level conditions, allowing fish to move from one pool to the next without having to jump. This structure can operate in a broad range of hydraulic and biological conditions, reducing the impacts of annual changes in water level (Katopodis and Williams) [3].

Rajaratnam et al. [7] conducted a crucial study on the hydraulics of VSFs. They investigated various configurations of VSF and determined the flow characteristics in seven geometry designs and four different geometric scales. Their results presented a dimensionless relation known as the characteristic discharge. Rajaratnam et al. [6] evaluated the performance of 18 fishway structures built in the United States, leading to the identification of three main and simple designs for fishway structures with vertical slots. Additionally, Wu et al. [16] studied fishway structure number 18 from Rajaratnam et al.'s [6] study and determined the likely flow patterns in slopes of 5%, 10%, and 20%. Rajaratnam et al. [7] established a linear relationship, expressed in Equation (1), between the characteristic discharge parameter of the flow and the relative depth parameter (y_0/s).

$$Q_* = \alpha(y_0/s) + \beta \quad (1)$$

where α and β are constant coefficients of the linear relationship between characteristic discharge and flow depth (y_0), and s is width of opening in slots of VSF.

Baharvand and Lashkar-Ara [17] modified the geometry configuration of C-type Meander fishways, i.e., a novel design of VSFs, presented by Stamm et al. [18]. They studied the effect of geometry scenarios on the dimensionless discharge of Modified Meander C-type Fishway (MMCF) using physical and numerical models. The unique geometry of MMCF shapes the mixing process within the structure's pools. This mixing process can enhance the flow's energy dissipation along the structure due to the fluid

friction effect, which increases the structure's efficiency, particularly for steep slopes. However, it is necessary to assess the ability of MMCF to accommodate a variety of fish species.

The present study endeavors to investigate the biological aspects of various geometric scenarios of MMCF for a critical slope of 20% through a combination of experimental and computational fluid dynamics models. Several slot opening ratios with and without modified baffle blocks will be employed to evaluate the effective parameters for designing and operating the MMCF. Fluid friction coefficient (C_f), and turbulent kinetic energy (TKE) are the target hydraulic parameters of the current study that were not investigated by Baharvand and Lashkar-Ara [17]. Moreover, the swimming speed of three synthetic Rainbow Trout (Oncorhynchus mykiss) fish species, with varying body lengths, will be calculated using empirical methods to assess their ability to safely navigate through the pools of the MMCF.

2 Materials and method

The study evaluated the hydraulic performance and biological suitability of the Modified Meander C-type Fishway by using physical and numerical models. The MMCF was designed to increase energy dissipation and ease of construction compared to vertical slot fishways. The physical model was built on a bed slope of 20% at the Jundi-Shapur University of Technology's Hydraulic Laboratory with a total length of 6.62 m and width of 1.31 m. The design is shown in Figure 1.

Figure 1(a) displays a perspective view of the model with C-type pools and pool radius R. The main channel and tailwater pool had a total length of 5.62 m. Three pools, numbers 8, 9, and 10, served as measuring stations to determine flow depth and depth-

averaged velocity. Pressure transducers were installed at the pool bed to measure total pressure and convert pressure fluctuations to mean flow depth using a digital data logger.

Once the mean flow depth is estimated by the pressure transducers, the depth-averaged velocity of the flow at the vertical slot cross-section is calculated using $\bar{V} = \frac{Q}{\overline{h_f} \times s}$, in which $\bar{V}$ is the depth-averaged velocity at slots of the MMCF, Q refers to the flow discharge obtained from an electromagnetic flowmeter installed in a pumping station, $\overline{h_f}$ is the average of 60-sec flow depth fluctuation at the slots of measuring pools, and s represents the width of opening at the slots. Figure 1(b) depicts a top view of the measuring pools in the MMCF, which were designed to study the potential flow patterns in the pools. Wooden baffle blocks designed with two height (h_b) scenarios were built and placed in the middle of the vertical slot openings to increase the submergence ratio and control the flow velocity inside the pools (Figure 1c). The design and measurement techniques used in the laboratory, as well as the operating scenarios, are described in detail by Baharvand and Lashkar-Ara [17].

Figure 2 depicts the complete process of the present study, from building the physical model to conducting CFD simulations and evaluating the ability of rainbow trout to navigate through the MMCF's pools.

According to Figure 2, the validation of the CFD model was carried out by comparing the results obtained from the physical model's velocity and depth measurements at the slots with numerical model. The friction coefficient in the modified meander c-type fishway pools was estimated using a combination of the experimental measurements and CFD model outputs. The CFD model simulation was used to evaluate the turbulent kinetic energy distribution in the pools of the MMCF and determine the safe zones for

fish. Lastly, the ability of three different sizes of rainbow trout to migrate through the MMCF was analyzed based on their propulsive energy and the fishway's geometry and flow conditions.

2.1 Fluid friction coefficient calculation

Rajaratnam et al. [7] proved the importance of friction coefficient in different designs of vertical slot fishways. Laboratory assessments at the measuring pools revealed that MMCF could create turbulent eddies while the flow passes through the structure pools. Therefore, each pool is expected to have more energy dissipation due to the turbulent regime with a lower fluid friction coefficient. Therefore, fluid friction coefficient parameter could be investigated as an effective hydrodynamic parameter controlling the shear stress generated between the flow in vertical slots and the water mass in downstream pool.

The fluid friction coefficient (C_f), i.e., a factor that determines the shear stress between different fluid layers, can be calculated using Equations (2) to (6).

$$\gamma R S_0 = \tau_0 \quad (2)$$

where γ is the specific weight of the fluid, τ_0 refers to the shear stress component, S_0 is the bed slope, and R is the ratio of the cross-sectional area of the main channel could be represented by Equation (3).

$$R = S_0 \bar{d}/(s + 2\bar{d}) \quad (3)$$

where $\bar{d}$ is the average depth of the flow.

Equation (4) is obtained by substituting Equation (3) with Equation (2) to determine the friction coefficient.

$$\rho g S_0 S\bar{d} = \tau_0(s + 2\bar{d}) \quad (4)$$

Equation (5) shows the relationship between shear stress and C_f in vertical slot fishways (Rajaratnam et al.) [7].

$$\tau_0 = C_f \frac{\rho V^2}{2} \quad (5)$$

The fluid friction coefficient for MMCF can be defined using Equation (6), which is obtained by substituting Equation (5) into Equation (4).

$$C_f = \frac{2gS_0\bar{d}}{V^2(1+2\bar{d}/s)} \quad (6)$$

Equation (6) is used to estimate the friction coefficient of MMCF for different geometry and discharge scenarios using both physical and CFD models.

2.2 Numerical simulations

In recent years, CFD models have been widely used in modeling the flow in fishways. This is due to the critical impact that flow characteristics have on fish behavior and fish habitat suitability indices. Many studies have utilized CFD models to study fishways, including those by Cea et al. [19], Barton et al. [20], Fu et al. [21], Mariner et al. [8], Mahmoudian et al. [22], Baharvand and Lashkar-Ara [17, 23].

2.2.1 Numerical model setup

In present study, Flow-3D (i.e., a widely used finite volume-based computational fluid dynamics model that simulates fluid- and heat-transfer problems) was used to simulate

flow in MMCF for various geometry scenarios. The model can incorporate a variety of solid geometry design cases, which makes it easier to import the geometry and embed the solid geometry model using the Fractional Area Volume Obstacle Representation (FAVOR) method (Hirt and Sicilian) [24], (Flow Science User's Manual) [25].

The Navier-Stokes equations, which are the primary equations solved by the Flow-3D model to simulate the flow field in various conditions, are presented in Equations (7-10). The Navier-Stokes equations are a set of three-dimensional mass and momentum conservation equations that are discretized using the Finite Volume Method (FVM). To model the turbulent regime in MMCF, the Flow-3D model employs the K-ε turbulence model, which has been used in the hydrodynamic modeling of fishways by various researchers, including Baharvand and Lashkar-Ara [23], Duguay et al. [26], and Mahmoudian et al. [22]. The solid geometry regions within the grids in the Flow-3D model are defined using the Fractional Area/Volume Obstacle Representation (FAVOR) method (Samani et al.) [27].

$$V_F \frac{\partial \rho}{\partial t} + \frac{\partial}{\partial x}(\rho u A_x) + \frac{\partial}{\partial y}(\rho v A_y) + \frac{\partial}{\partial z}(\rho w A_z) = 0 \quad (7)$$

$$\frac{\partial \mathrm{u}}{\partial t} + \frac{1}{\mathrm{V}_F}\left\{uA_x \frac{\partial \mathrm{u}}{\partial \mathrm{x}} + vA_y \frac{\partial \mathrm{u}}{\partial \mathrm{y}} + wA_z \frac{\partial \mathrm{u}}{\partial \mathrm{z}}\right\} = -\frac{1}{\rho}\frac{\partial p}{\partial x} + G_x + f \quad (8)$$

$$\frac{\partial \mathrm{v}}{\partial t} + \frac{1}{\mathrm{V}_F}\left\{uA_x \frac{\partial \mathrm{v}}{\partial \mathrm{x}} + vA_y \frac{\partial \mathrm{v}}{\partial \mathrm{y}} + wA_z \frac{\partial \mathrm{v}}{\partial \mathrm{z}}\right\} = -\frac{1}{\rho}\frac{\partial p}{\partial y} + G_y + f \quad (9)$$

$$\frac{\partial \mathrm{w}}{\partial t} + \frac{1}{\mathrm{V}_F}\left\{uA_x \frac{\partial \mathrm{w}}{\partial \mathrm{x}} + vA_y \frac{\partial \mathrm{w}}{\partial \mathrm{y}} + wA_z \frac{\partial \mathrm{w}}{\partial \mathrm{z}}\right\} = -\frac{1}{\rho}\frac{\partial p}{\partial z} + G_z + f \quad (10)$$

where A_x, A_y, and A_z refer to the Cartesian system's desired fluid volume of the element's free surface component. G and f are the main gravitational component and gravity from the viscosity of the fluid, respectively. u, v, and w are velocity components in x, y, z directions, respectively. More information on the Navier-stocks equation and computational process would be found at Flow Science (2018).

Figure 3 depicts the simulated flow in MMCF for a specified discharge of Q = 37 l/s and s/R = 0.2. The inlet boundary condition was set to the flow discharge, while the outlet and upper mesh plane were assigned a zero-pressure boundary condition. To reflect the free surface boundary condition with air-water interaction, the Volume of Fluid (VOF) method was utilized, which determines the volume fraction with values ranging from 0 to 1 for empty and fully filled cells, respectively (Stamou et al.) [28].

The sidewalls and bottom of the structure were assigned wall boundary conditions, with an average roughness height of 0.3 mm (concrete wall). The computational mesh domain was discretized to the optimal finest mesh cells for modeling, and the exact number of mesh cells for each model was determined based on specific geometry configuration scenarios, such as s/R and h_b/R. The mesh sensitivity test was conducted for all models, and the finest rectangular mesh domain with 590,000 cubic cells was selected for the entire control volume after consideration of all results. In accordance with the Froude similarity, the prototype geometry scale was reduced by a factor of four (scale 1:4). The pool's radius is R = 0.1 m for all CFD scenarios.

The capacity of the pools in the MMCF determines the range of discharge that is allowed to prevent overtopping and ensure a minimum flow depth sufficient for the

passage of fish species. Table 1 presents the various discharge, baffle height, and opening ratios that were considered in the numerical modeling for different models.

2.2.2 Turbulent Kinetic Energy in MMCF pools

The swimming capability and behavior of fish species are closely related to the hydraulic conditions (speed, depth) and the turbulence structures formed in the pools of the fishway (Shahabi et al.) [29]. The Total Kinetic Energy (TKE) was calculated using Equation 11, which employs the velocity fluctuation components in every direction in a CFD model (Rodi) [30], (Silva et al.) [31].

$$TKE = \frac{1}{2}(\overline{(u')^2} + \overline{(v')^2} + \overline{(w')^2}) \quad (11)$$

where u', v', w' are flow velocity fluctuation components in longitudinal (x), transverse (y), and vertical (z) directions.

2.2.3 Validation of the numerical model

The depth-averaged velocity (V□) and the mean flow depth (d□) at the slots of the MMCF measuring pools were determined using both experimental measurements and a CFD model. The discharge observed in the physical model was compared to the discharges obtained from the CFD model to evaluate the accuracy of the flow simulation for different geometric scenarios. Figure 4 illustrates the comparison of discharge between the physical and numerical models for s/R = 0.1 and three different baffle height scenarios (h_b/R = 0, 0.1, 0.2) in pool number 8.

The CFD model demonstrates high accuracy for each baffle height scenario, with R-squared values ranging from 0.94 to 0.96 for s/R = 0.1 (Figure 4). Figures 5 and 6 show

the comparison of measured and simulated discharge for s/R = 0.2 and 0.3 with a minimum R^2 =0.96 that proves the precision of CFD model.

Furthermore, the average water surface elevation in the middle of the measuring station (at the center of the slot in pool number 8) is compared to the result from the CFD model at the same location. The Mean Error (ME) of the water surface elevation for s/R = 0.1 was determined to be 5.69%. The mean error of the simulated water surface elevation for s/R = 0.2 and 0.3 is 8.12% and 9.05%, respectively. It is important to note that factors such as mesh size, simplification assumptions, and inaccuracies in laboratory measurements could result in some discrepancy between the CFD model and physical model results. Nevertheless, the low mean error and favorable R-squared statistical metrics demonstrate that the CFD model is validated and can be utilized to evaluate various hydrodynamic variables of flow in MMCF, including TKE and C_f.

2.3 Fish swimming capabilities and biological properties

Fish species have two types of muscles - red and white - that affect their swimming speed and time to exhaustion, i.e., the maximum time a fish can swim without rest (Behlk) [32]. The white muscles can produce swimming speeds four times greater than the red muscles, but tire much more quickly. This difference in performance makes the white muscle critical in fishway design, especially in high-velocity areas such as the opening slots of vertical slot fishways. By analyzing the swimming behavior and forces on the fish body, it is possible to determine the suitability of each fishway design for a specific fish species (Behlk) [32,33].

2.3.1 Dynamics of fish swimming

According to the study conducted by Behlk et al. [32,33], three main forces act on the body of fish species while swimming in natural streams: gravitational, virtual mass, and drag. These forces are depicted in Figure 7, where the direction of each force on the fish body is illustrated.

The three main forces acting on fish bodies during swimming in natural streams are gravitational force (F_G), virtual mass force (F_{vm}), and profile drag (F_D). F_G is due to weight and buoyant force and acts in the opposite direction to the fish's movement path. F_{vm} is generated by both red and white muscles when the fish needs to swim faster. F_D is the result of skin friction and pressure and is the hardest force to measure directly. Figure 7(b) and (c) show the direction of F_{vm} and F_D on the fish body, respectively, and Table 2 lists the governing equations used to estimate these forces.

2.3.2 Fish propulsive energy calculations

The propulsive force required for a fish to successfully navigate through a fish passage is determined by the total of various forces that impact its body. These forces include gravitational force (F_G), virtual mass force (F_{vm}), and profile drag (F_D), which are represented in Equation 15.

$$F_p = F_G + F_{vm} + F_D \quad (15)$$

where F_p is the net propulsive force acting on the fish body.

According to a study by Behlk [32], the net propulsive force (F_p) acting on the fish body must be countered by an equal amount of energy generated by the fish in order to swim upstream. To determine the net propulsive power (P_{wr}) for each fish class, the swimming speed of the fish relative to the surrounding water should be calculated using Equation (16).

$$P_{wr} = F_p \times V_{fw} \quad (16)$$

Rainbow trout was selected as the main fish species of the present study. The physical characteristics of the rainbow trout are collected from available datasets and will be discussed in the next section. Equation 17 represents the net propulsive energy (E_p) required for a fish to migrate upstream in open channel (Behlk) [32, 33].

$$E_p = P_{wr} \frac{L_c}{V_f} \quad (17)$$

where L_c refers to the critical length of fish swimming path, that is considered to be total length in present study (TL). In the present study, physical characteristics of Rainbow trout were utilized to examine the factors that influence the swimming capability of this specific fish species. This was done by considering three hypothetical body lengths that reflect the age of the fish.

2.4 Rainbow trout characteristics

Rainbow trout, also known as "*Oncorhynchus mykiss*", are a vital species in North America and Canada with a historical range from Alaska to Mexico. They are a type of cold-water fish that can thrive in various environments with ideal temperatures between 12.7 and 23.8 degrees Celsius. However, factors such as changes in water quality, rising temperatures, and the loss of riverside vegetation and soil erosion have led to a decline in their distribution. Changes in water quality and drought (Maymandi et al.) [34], increased average temperature and drought (Hassanzadeh et al.) [35], loss of vegetation in riversides, soil erosion (Baharvand et al.) [36], (Kabir et al.) [37], etc., are examples that led to a significant reduction in the suitability of aquatic habitat distribution (Ahmari et al.) [38]. Also, human activities such as dams and bridges constructions are altering the

habitat conditions for the migration of native aquatic species, a crucial part of their life cycle (Baharvand et al.) [39], (Fathinezhad et al.) [40], (Nasseri and Hummel) [41], (Ahmari et al.) [38,42]. As a result of these alterations to the rainbow trout habitat, nine types of the species have been listed on the federal endangered species list (FWS) and a comprehensive assessment of fish migratory facilities is required to mitigate the effect of human made constructions on aquatic habitat.

Hunter and Mayor [43] found that fish length is a critical factor in fish behavior and used a nonlinear regression relationship between fish length and time to exhaustion to estimate fish swimming speed (Equation 18). In the present study, the swimming speed of hypothetical rainbow trout fish species were estimated using Equation (18).

$$V_f = \alpha L_f^{\beta} t^{\zeta} \quad (18)$$

where α , β, and ζ represent the regression coefficient constants and would differ based on fish species. L_f represents the length of fish, and t is the time to exhaustion. In the present study, the swimming speed constants and the rainbow trout's minimum, mean, and maximum length were obtained from Furniss et al.'s [44].

In the present study, the total length (TL) of rainbow trout was used as the primary measure of body length (Figure 8). Table 3 presents the physical characteristics of three hypothetical rainbow trout with different body lengths selected to reflect the range of rainbow trout length measurements. The burst swimming speed was calculated for each class of rainbow trout using Equation (18), with a time to exhaustion of 20 sec and the burst swimming coefficients listed in Table 3.

In the study by Larinier [45], it was established that the volumetric energy dissipation in fishway pools should be below 200 W/m3 for salmonids and 150 W/m3 for cyprinids

to be considered acceptable. The present study calculates the net propulsive energy for each class of hypothetical rainbow trout for different energy dissipation rates using Equation (19) (Baki) [46], (Towler et al.) [47].

$$E_v = \frac{\gamma Q \Delta H}{Ad} \quad (19)$$

where E_v represents the volumetric energy dissipation, γ refers to the specific weight of water, Q is flow discharge, ΔH is the head loss for each pool of MMCF, A is the area of the pool, and d is the average depth of water. The following section will variation in the propulsive energy of fish species for varying energy dissipation rates.

3 Results and Discussion

3.1 Effect of the opening ratio (*s/R*) on the friction coefficient (C_f)

Based on experimental observations, a high-velocity flow jet will be shaped in slots of MMCF, which will mix with the subsequent flow zone in the pool. This mixing process can result in the dissipation of energy from the upstream high-velocity flow due to existing friction between flow layers in mixing process. Consequently, in MMCF, the friction coefficient is a crucial factor, particularly when the flow is turbulent.

Figure 9 shows the relationship between the fluid friction coefficient (Cf) and the relative flow depth for $h_b/R = 0$ (i.e., corresponds to the absence of baffle blocks), where h_b/R represents the ratio of the average flow depth to the slot's opening width (s). The results presented in Figure 9 illustrate that the fluid friction coefficient (Cf) varies between 0.02 to 0.06 for different relative depth scenarios, which span from negligible amounts to a depth ratio of d/s = 7.84 for a flow rate of Q = 24 l/s.

Figure 9 employs more than four discharge scenarios, which are also used in the CFD model (as listed in Table 1), to represent the laboratory tests. To enhance the accuracy of the regression trends for the friction coefficient, some discharge scenarios are linearly interpolated between the values listed in Table 1. The experimental tests used discharges that varied between the minimum (Q1) and maximum (Q4) discharges stated in Table 1.

Figures 10 and 11 depict the variation of C_f with respect to the relative depth ratio (d/s) for h_b/R = 0.1 and 0.2, respectively, with different opening ratios. It is worth mentioning that the highest value of d/s for each s/R scenario in Figures 9, 10, and 11 represents the maximum discharge scenario for the C_f variation plots. Similarly, the lowest value of the relative depth ratio corresponds to the minimum discharge scenario for each geometry listed in Table 1.

As shown in Figure 9, the fluid friction coefficient (Cf) exhibits a decreasing trend across all opening ratios of MMCF. This implies that for the range of discharges considered in this study, a higher relative depth ratio (i.e., corresponding to a higher discharge scenario) results in a lower friction coefficient in MMCF pools.

Based on the laboratory observations, a submerged jet is formed in the pools of MMCF for an average value of d/s = 6.15, 3.2, and 1.7 for h_b/R = 0.1, 0.2, and 0.3, respectively. However, for low discharge scenarios, the mixing process is not visibly detectable in the measuring pools of MMCF for hb/R = 0, due to the highly turbulent flow regime. Figure 9 demonstrates that for all scenarios, the maximum C_f occurs at the d/s for each opening ratio. In contrast, C_f exhibits a decreasing nonlinear trend for higher relative flow depth, which results in a higher rate of turbulent eddies created in the pools

due to the mixing process. This observation is based on a qualitative comparison of image sequences taken from the flow pattern over Pool no. 8.

Increasing the opening ratio from s/R=0.1 to s/R=0.3 shifts the values of fluid friction coefficient to lower d/s of less than C_f =0.035 (as shown in Figure 9) for the specified discharge range. This indicates that for higher s/R values, the friction coefficient is reduced due to the dissipation of energy caused by the turbulent regime in the pools. In other words, achieving the same friction coefficient for s/R=0.1 and s/R=0.3 requires approximately six times higher average relative depth ratio for the specified discharge range.

The maximum friction coefficient in Figure 10 occurs at s/R = 0.2 and a discharge of Q = 26 l/s, with all other baffle height ratios having a lower maximum C_f than s/R = 0.2 (as seen in Figures 9 and 10). Therefore, s/R = 0.2 provides the highest friction coefficient, which are 0.062, 0.415, and 0.718, for h_b/R = 0, 0.1, 0.2, respectively. Figures 10 and 11 also show less variation in C_f compared to Figure 9 for s/R = 0.1, indicating that baffle blocks significantly increase the friction coefficient compared to h_b/R = 0.

In Figure 12, a qualitative assessment of two flow pattern variations in MMCF pools are presented: one with no baffle (h_b/R=0) and s/R=0.1 (Figure 12a), and the other with s/R=0.2 (Figure 12b) with having a similar d/s=2.54. The discharge for s/R=0.1 and 0.2 are Q=13 l/s and Q=20 l/s, respectively. The creation of a turbulent flow zone due to the submerged flow jet can be observed in Figure 12(b).

Besides friction coefficient, the velocity fluctuations in different directions can also affect the swimming ability and stability of fish by creating resistant forces. The

Turbulent Kinetic Energy (TKE) parameter will be discussed in the next section as an important factor to evaluate the impact of velocity fluctuation components on fish species swimming capability.

3.2 Turbulent Kinetic Energy in MMCF pools

The TKE variation through the largest Pool's Middle Axis (PMA) in Pool 8 was evaluated using the numerical model results. Figure 13 illustrates the TKE changes along the PMA for three opening ratios (s/R = 0, 0.1, 0.2) and the no baffle block scenario (h_b/R = 0) at a depth of 0.5d (where d represents the average flow depth at pool). Figures 13(a-c) demonstrate that the range of turbulent kinetic energy for the no baffle block scenario (h_b/R=0) is from negligible amounts near the walls at PMA=0 and PMA=1, to a maximum of 0.48 m^2/s^2, 0.402 m^2/s^2, and 0.32 m^2/s^2 for s/R = 0, 0.1, 0.2, respectively. Additionally, for all opening ratios, the TKE increases once PMA>0, indicating the high turbulent kinetic energy of the incoming jet from pool no. 7 to pool no. 8 (illustrated in Figure 12).

Figure 13(a) shows that TKE ranges from 0.37 m^2/s^2 to 0.48 m^2/s^2 between PMA=0 to PMA=0.3, decreases to 0.2 m^2/s^2 for Q=13 l/s, and a low of 0.162 m^2/s^2 for Q=24 l/s. TKE remains relatively close to 0.2 m^2/s^2 for all discharge scenarios within a PMA range from 0.2 to 0.93, as seen in all scenarios in Figure 13.

High turbulent kinetic energy regions can be identified when PMA = 0.93, as there is a noticeable increase in TKE for all discharge scenarios near this point. Therefore, around 14% of the PMA in each scenario represents the high TKE zones that correspond to the high flow velocity jets observed in laboratory experiments. The maximum TKE for

PMA > 0.93 is approximately 0.25 J/kg for all discharge scenarios. TKE becomes negligible again near the walls of the MMCF structure (PMA≈1).

Figure 13(a) shows that increasing the opening ratio from s/R = 0.1 to 0.2 and 0.3 results in a decrease in maximum TKE, but an increase in discharge scenarios. Thus, the MMCF with higher opening ratios may provide safer zones for migratory fishes due to less turbulent kinetic energy variations. TKE for s/R = 0.2 varies from 0.13 to a maximum of 0.22 J/kg at PMA = 0.97. Figure 13(c) depicts that the high flow jet for s/R = 0.3 ranges from PMA = 0 to 0.08, possibly due to low contraction effects on the flow (greater opening ratio). The middle part of the pool at s/R = 0.3 shows higher TKE values than s/R = 0 and s/R = 0.1, indicating an unsafe zone for some migratory fish species.

It appears that the installation of baffle blocks at the middle of the opening slots reduces the TKE significantly, as shown in Figures 14 and 15 for h_b/R=0.1 and 0.2, respectively. For PMA > 0.3, the TKE is less than 0.1 m^2/s^2 for an opening ratio of s/R = 0.1 and h_b/R=0.1 and 0.2, while for s/R=0.2 and s/R=0.3, the TKE ranges from a low of 0.11 m^2/s^2 to a high of 0.23 m^2/s^2. The TKE fluctuations for PMA > 0.3 for both h_b/R=0.1 and 0.2 are much less than h_b/R=0 shown in Figure 13.

According to the TKE variation discussed above, the decrease in TKE due to the use of baffle blocks may improve the safety and resting areas for migratory fish species. The swimming abilities of rainbow trout will be investigated for all mentioned geometry and discharge scenarios in the following section. Engineers and designers can refer to the TKE graphs to estimate the possible resting pool size based on the specific biological criteria of the fish species. By estimating the safe zones, the fishway pools can be

designed optimally to achieve a high migration rate while minimizing fatigue and risk to the fish's health.

3.3 Migratory Capabilities of Rainbow Trout

After acquiring biological data on rainbow trout from Furniss et al. [44] and creating three hypothetical classes of rainbow trout based on body length and swimming capabilities, the fish species' biological power is employed to evaluate the propulsive energy available for various MMCF design scenarios. Figures 16 to 18 show the computed propulsive energy of the three hypothetical Rainbow trout classes for passing the pools of MMCF with different opening ratios (s/R = 0.1, 0.2, and 0.3). The propulsive energy required for the three hypothetical Rainbow trout classes to pass through the pools of MMCF with different opening ratios (s/R = 0.1, 0.2, and 0.3) is presented in Figures 16 to 18, which was calculated using Equation 17.

It can be observed from Figures 16 to 18 that the energy dissipation rate remains below 150 W/m3 for all discharge scenarios. This is considered suitable for Salmonid fish species, which includes Rainbow trout, based on the criteria established by Larinier [45]. Figure 16 illustrates the propulsive energy for the hypothetical Rainbow trout fish species in the MMCF with s/R = 0.1 and hb/R = 0, 0.1, and 0.2. Each trendline represents the energy produced by the fish using burst velocity for the discharge scenarios outlined in Table 1. The lowest volumetric energy dissipation occurs at the lowest discharge scenario, while the highest discharge scenario for each scenario results in the greatest potential volumetric energy.

When comparing the potential volumetric energy dissipation of the flow in the measuring pool to the available propulsive energy, it was found that rainbow trout class 1

may not generate the same amount of propulsive energy as is dissipated energy in the pools for s/R = 0.1 and h_b/R = 0 and 0.1 (Figure 16) for the corresponding discharge rates (Table 1). As can be seen, the rainbow trout class 1 could generate greater propulsive energy (E_p = 21 *J*) than the pools' dissipated energy after replacing the baffle block with h_b/R = 0.2.

Furthermore, rainbow trout classes 2 and 3 exhibit similar propulsive energy values for various volumetric energy dissipation levels at s/R=0.1, regardless of the discharge scenario. Higher discharge rates result in greater propulsive energy due to the greater availability of volumetric energy dissipation in the MMCF pools. The migration trends in all cases demonstrate the impact of baffle blocks in reducing volumetric energy. In Figures 16 to 18, the red trendlines correspond to the absence of baffle blocks (h_b/R=0), the blue trendlines represent h_b/R=0.1, and the black trendlines illustrate the changes in propulsive energy for different energy dissipation rates at h_b/R=0.2.

The hydraulic conditions for ensuring a secure fish passage are different for s/R=0.1 compared to higher slot opening ratios (s/R=0.2 and 0.3), as shown in Figures 17 and 18. Higher minimum discharges are needed to maintain suitable hydrodynamic criteria for fish species, and the volumetric energy dissipation of the MMCF pools increases with the flow discharge. Rainbow trout class 1 may face swimming difficulties for all baffle block height ratios (h_b/R=0, 0.1, 0.2) due to the increased volumetric energy dissipation. However, the maximum volumetric energy dissipation criteria (E_v < 200) indicate general suitability. Rainbow trout classes 2 and 3 produce propulsive energy ranging from 45 J to 132 J for the specified discharge rate for s/R = 0.2. The maximum height of

the modified baffle blocks (h_b/R) results in the lowest propulsive energy for creating a safe fish passage, as seen in Figure 16.

The physical characteristics assumed for each fish class result in class 3 producing more propulsive energy than classes 1 and 2. For example, at a volumetric energy of 60 W/m3, class 3 generates 2.4 times more propulsive energy than class 1, as shown in Figure 17. However, increasing the baffle block height to h_b/R=0.1, 0.2 causes the propulsive energy diagrams for fish classes 2 and 3 to merge.

Similar to the propulsive energy produced by fish species for *s/R* = 0.2 in Figure 17, rainbow trout classes 2 and 3 will be able to pass the fishway's pools for all baffle height scenarios with *s/R* = 0.3 (Figure 18). The propulsive energy of the fish class 1 for *s/R* = 0.3 ranges from 28 *J* to 64 *J*, which is relatively less than the available volumetric energy at pools of MMCF, which ranges from 32 *J* to 88 *J*.

Comparing the propulsive energy variations in Figures 16 to 18 showed the ability of fish species to generate the appropriate potential energy that each fish class could generate due to the hydraulic characteristics of the MMCF using the burst swimming condition. Rainbow trout 1 represents less ability to produce propulsive energy in the pools due to less muscular ability to generate the burst swimming speed than classes 2 and 3 with higher weight and length. Also, the propulsive energy is increased for larger opening ratios so that the biological energy needed for fish to pass pools ranges from 15 J to 16 J for s/R = 0.1, but it ranges between 28 *J* to 166 *J* for *s/R* = 0.3. Overall, the volumetric energy dissipation for all geometric scenarios of the study was in the acceptable range for salmonid fish species. However, in some cases, the fish species with

a smaller length and weight produced lower propulsive energy generated by the white muscles.

4 Conclusion

The Modified Meander C-type Fishway (MMCF) was previously introduced by Baharvand and Lashkar-Ara [17] as a vertical slot fishway for safely passing fish species upstream. However, the hydraulic characteristics of the flow in the pools of the structure, including fluid friction coefficient and turbulent kinetic energy, have not been thoroughly studied. This study aimed to comprehensively evaluate these parameters using physical and numerical modeling approaches. The fishway's bed slope remained constant (20%), and wooden baffle blocks of different heights were used as modification elements to create safe zones for different opening slot ratios.

Turbulent Kinetic Energy distribution and fluid friction coefficient variation in measuring pool were obtained and presented using the computational fluid dynamic model for different discharge and geometry scenarios through a measuring station pool. The fluid friction is ranged between 0.02 to 0.06 for different relative depth scenarios for $h_b/R = 0$ with a maximum d/s = 7.84 for Q = 24 l/s. Also, it is shown that for all discharge scenarios, increasing the opening ratio from s/R =0.1 to s/R = 0.3 shifts the C_f values to the lower d/s ranges less than $C_f = 0.035$ for the specified discharge range. It is shown that the maximum friction coefficient obtained for greatest opening ratio. The TKE distribution graphs for different discharge and geometry scenarios through the longest path in the measuring pool of the MMCF were investigated using the line probe technique at an average depth of 0.5d. It is revealed that the TKE is reduced significantly

once the baffle blocks installed at the opening slots of the MMCF that provides safer resting zones in pools for migratory fish species.

The study also estimated the swimming speeds and propulsive energy of three synthetic classes of rainbow trout in the MMCF, comparing them with the potential energy dissipation in the measuring pool. Overall, the MMCF was found to be effective for passing fish species of different classes, although there were concerns about the ability of small rainbow trout to pass in certain scenarios (Class 1). Findings of present study can be used for hydraulic design of the MMCF with consideration of the biological needs of fish species by relevant organizations and designers. Due to limitations in the laboratory facilities, the study was unable to include a wider range of flow discharge scenarios. It is recommended to expand the range of discharge scenarios to conduct a more comprehensive analysis that considers a variety of possible discharges.

Data availability: Some or all data, models, or codes supporting this study's findings are available from the corresponding author upon reasonable request.

5 Acknowledgment

The authors would like to thank Jundi-Shapur University of Technology for their support during physical and numerical modeling.

6 References

[1] Clay, C. H., and Eng., P., "*Design of Fishways and Other Fish Facilities"*. CRC Press (2017).

[2] Weibel, D., and Peter, A. "Effectiveness of different types of block ramps for fish upstream movement." *Aquatic Sciences*, 75(2), 251–260 (2013).

[3] Katopodis, C., and Williams, J. G. "The development of fish passage research in a historical context." *Ecological Engineering*, 48, 8–18 (2012).

[4] Baki, A. B. M., Zhu, D. Z., and Rajaratnam, N. "Mean Flow Characteristics in a Rock-Ramp-Type Fish Pass." *Journal of Hydraulic Engineering*, 140(2), 156–168(2014).

[5] Katopodis, C., Kells, J. A., and Acharya, M. "Nature-Like and Conventional Fishways: Alternative Concepts?" *Canadian Water Resources Journal*, 26(2), 211–232 (2001).

[6] Rajaratnam, N., Katopodis, C., and Solanki, S. "New designs for vertical slot fishways." *Canadian Journal of Civil Engineering*, 19(3), 402–414 (1992).

[7] Rajaratnam, N., Van der Vinne, G., and Katopodis, C. "Hydraulics of Vertical Slot Fishways." *Journal of Hydraulic Engineering*, 112(10), 909–927 (1986).

[8] Marriner, B. A., Baki, A. B. M., Zhu, D. Z., Cooke, S. J., and Katopodis, C. "The hydraulics of a vertical slot fishway: A case study on the multi-species Vianney-Legendre fishway in Quebec, Canada." *Ecological Engineering*, 90, 190–202 (2016).

[9] Decker, L. F. "Fishways in Maine. Pamphlet, Maine Department of Inland Fisheries and Game", Information and Education Division (1956).

[10] Noonan, M. J., Grant, J. W. A., and Jackson, C. D. "A quantitative assessment of fish passage efficiency." *Fish and Fisheries*, 13(4), 450–464 (2012).

[11] Bunt, C. M., Castro-Santos, T., and Haro, A. "Performance of Fish Passage Structures at Upstream Barriers to Migration." *River Research and Applications*, 28(4), 457–478 (2012).

[12] DVWK. Fish passes-Design, dimensions and monitoring. Published by the Food and Agriculture Organization of the United Nations in arrangement with German. Association for Water Resources and Land Improvement as DVWK-Merkblatt (2002).

[13] Puertas, J., Cea, L., Bermúdez, M., Pena, L., Rodríguez, Á., Rabuñal, J. R., Balairón, L., Lara, Á., and Aramburu, E. "Computer application for the analysis and design of vertical slot fishways in accordance with the requirements of the target species." *Ecological Engineering*, 48, 51–60 (2012).

[14] Quaranta, E., Katopodis, C., and Comoglio, C. "Effects of bed slope on the flow field of vertical slot fishways." *River Research and Applications*, rra.3428 (2019).

[15] Baki, A. B. M., and Azimi, A. H. "Hydraulics and design of fishways II: vertical-slot and rock-weir fishways." *Journal of Ecohydraulics*, 1–13 (2021).

[16] Wu, S., Rajaratnam, N., and Katopodis, C. "Structure of Flow in Vertical Slot Fishway." *Journal of Hydraulic Engineering*, 125(4), 351–360 (1999).

[17] Baharvand, S., and Lashkar-Ara, B. "Hydraulic design criteria of the modified meander C-type fishway using the combined experimental and CFD models." *Ecological Engineering*, 164, 106207 (2021).

[18] Stamm, J., Helbig, U., and Zimmermann, R., "Hydraulic characteristics of meander-type fish passes." In: Proceedings of the 36th IAHR World Congress 28 June - 3 July, 2015, The Hague, The Netherlands, pp. 1–13, (2015).

[19] Cea, L., Pena, L., Puertas, J., Vázquez-Cendón, M. E., and Peña, E. "Application of Several Depth-Averaged Turbulence Models to Simulate Flow in Vertical Slot Fishways." *Journal of Hydraulic Engineering*, 133(2), 160–172 (2007).

[20] Barton, A. F., Keller, R. J., and Katopodis, C. "Verification of a numerical model for the prediction of low slope vertical slot fishway hydraulics." *Australasian Journal of Water Resources*, 13(1), 53–60 (2009).

[21] Fu, J., Li, J., An, R., Mao, X., Yi, W., "Study of creating vertical slot fishway flow field based on swimming ability of Schizothorax prenanti. " J. Sichuan Univ. Eng. Sci. Ed. 45 (3), 12–17 (2013).

[22] Mahmoudian, Z., Baharvand, S., and Lashkar-ara, B., "Investigating the Flow Pattern in Baffle Fishway Denil Type." Journal of Irrigation Science and Engineering. 42 (3), 179–196 (2019). Retrieved from: https://jise.scu.ac.ir/article_14644_4c35f29758d3bf63276e022c54e1adec.pdf?lang=en

[23] Baharvand, S., and Lashkar-Ara, B. "Determining the Effective of Resting Pool Area in Vertical Slot Fishways Type 1 to Pass Chinook Salmon." *Journal of Civil and Environmental Engineering*, 48(4), 1–12 (2019).

[24] Hirt, C., and J. Sicilian. "A porosity technique for the definition of obstacles in rectangular cell meshes." *In Proc., 4th Int. Conf. Ship Hydrodynamics*. Washington, DC: National Academy of Sciences (1985).

[25] Flow Science, Inc., Santa Fe, NM, USA. FLOW-3D® Version 12.0 User's Manual (2018) [Online]. Accessed on: Feb. 3, (2019).

[26] Duguay, J.M., Lacey, R.W.J. and Gaucher, J., "A case study of a pool and weir fishway modeled with OpenFOAM and FLOW-3D. " *Ecological engineerin*g, 103, pp.31-42 (2017).

[27] Samani, Z. A., Baharvand, S., and Davis, S. "Calibration of Stage–Discharge Relationship for Rectangular Flume with Central Cylindrical Contraction." *Journal of Irrigation and Drainage Engineering*, 147(8), 06021006 (2021)..

[28] Stamou, A. I., Mitsopoulos, G., Rutschmann, P., and Bui, M. D. "Verification of a 3D CFD model for vertical slot fish-passes." *Environmental Fluid Mechanics*, 18(6), 1435–1461 (2018).

[29] Shahabi, M., Ghomeshi, M., Ahadiyan, J., Mohammadian, T., and Katopodis, C. "Do fishways stress fish? Assessment of physiological and hydraulic parameters of rainbow trout navigating a novel W-weir fishway." *Ecological Engineering*, 169 (2021).

[30] Rodi, W. "Turbulence Models and Their Application in Hydraulics: A State-of-the-Art Review", 3rd edition. (2017). https://doi.org/10.1201/9780203734896.

[31] Silva, A. T., Katopodis, C., Santos, J. M., Ferreira, M. T., and Pinheiro, A. N. "Cyprinid swimming behaviour in response to turbulent flow." *Ecological Engineering*, 44, 314–328 (2012).

[32] Behlke, C.E., "Power and energy Implications of passage structures for fish. *Fisheries Bioengineering Symposium.*" *AFS Symposium*, pp. 289-298 (1991).

[33] Behlke, Charles E., Douglas L. Kane, Robert F. McLean, and Michael D. Travis. "Fundamentals of culvert design for passage of weak-swimming fish." Final Report, Alaska, DOT&PF, Fairbanks, AK, FHWA-AK-RD-90-10, February, 1991, 177 p, (1991).

[34] Maymandi, N., Hummel, M. A., and Zhang, Y. "Compound Coastal, Fluvial, and Pluvial Flooding During Historical Hurricane Events in the Sabine–Neches Estuary, Texas." *Water Resources Research*, 58(12) (2022).

[35] Hassanzadeh, Y., Ghazvinian, M., Abdi, A., Baharvand, S., and Jozaghi, A. "Prediction of short and long-term droughts using artificial neural networks and hydro-meteorological variables." *Atmospheric and Oceanic Physics*, (2020).

[36] Baharvand, S., Ahmari, H., and Taghvaei, P. "Developing a Lagrangian sediment transport model for open channel flows." *International Journal of Sediment Research*. (2023). https://doi.org/10.1016/j.ijsrc.2022.09.003

[37] Kabir, S. M. I., Ahmari, H., and Dean, M. "Experimental study to investigate the effects of bridge geometry and flow condition on hydrodynamic forces." *Journal of Fluids and Structures*, 113, 103688, (2022).

[38] Ahmari, H., Pebworth, M., Baharvand, S., Kandel, S., and Yu, X. "Development of an ArcGIS-Pro Toolkit for Assessing the Effects of Bridge Construction on Overland Soil Erosion." *Land*, 11(9), 1586 (2022). https://doi.org/10.3390/land11091586

[39] Baharvand, S., Rezaei, R., Talebbeydokhti, N., Nasiri, R., and Amiri, S. M. "Investigation of Energy Dissipation Rate of Stepped Vertical Overfall (SVO) Spillway Using Physical Modeling and Soft Computing Techniques." *KSCE Journal of Civil Engineering*, 26(12), 5067–5081 (2022). https://doi.org/10.3390/app10072552

[40] Fathinezhad, A., Jafari, N. H., Oldenburg, C. M., and Caldwell, M. D. "Numerical investigation of air intrusion and aerobic reactions in municipal solid waste landfills." *Waste Management*, 147, 60–72 (2022).

[41] Naseri, K., and Hummel, M. A. "A Bayesian copula-based nonstationary framework for compound flood risk assessment along US coastlines." *Journal of Hydrology*, 610, 128005 (2022).

[42] Ahmari, H., Baharvand, S., and Pebworth, M. "Developing an ArcGIS Pro Toolkit for Assessing Bridge Construction Effects on Sediment Regime and Aquatic Habitat ." 20th *Iranian Hydraulic Conference*, Gorgan University of Agricultural Sciences and Natural Resources, Gorgan, Iran (2021).

[43] Hunter, L., Mayor, A. "Analysis of Fish Swimming Performance Data." Unpublished Report. Vol. I (1986).

[44] Furniss, M., M. Love, S. Firor, K. Moynan, A. Llanos, J. Guntle, and R. Gubernick. "FishXing: software and learning systems for fish passage through culverts, version

3.0." U.S. Forest Sevice, San Dimas Technology and Development Center, San Dimas, California, (2006).

[45] Larinier, M. "Pool Fishways, Pre-Barrages and Natural Bypass." *Bulletin Français de la Pêche et de la Pisciculture*, (364 supplément), 54–82 (2002).

[46] Baki, A. B. M., Zhu, D. Z., Harwood, A., Lewis, A., and Healey, K. "Rock-weir fishway II: design evaluation and considerations." *Journal of Ecohydraulics*, 2(2), 142–152 (2017).

[47] Towler, B., Mulligan, K., and Haro, A. "Derivation and application of the energy dissipation factor in the design of fishways." *Ecological Engineering*, 83, 208–217 (2015).

[48] Webb, P. W., "Hydrodynamics and energetics of fish propulsion. " Bulletin of Fish. Res. Bd. of Can., Bull. 190, Ottawa, Canada (1975).

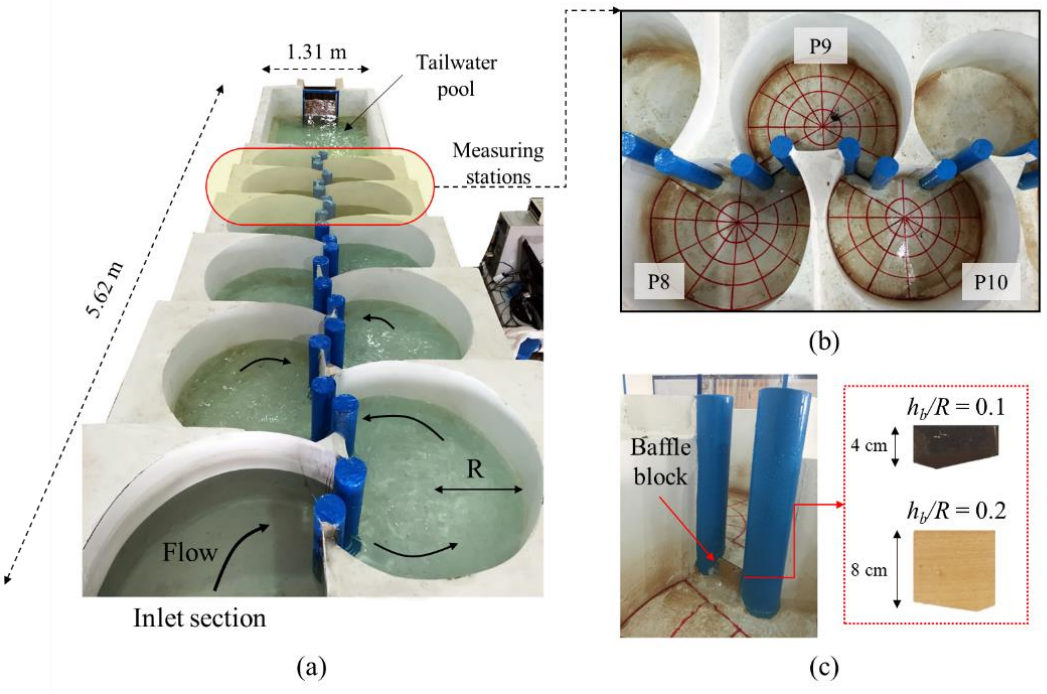

Figure 1. The Schematic of the Laboratory System Implemented in the Present Study

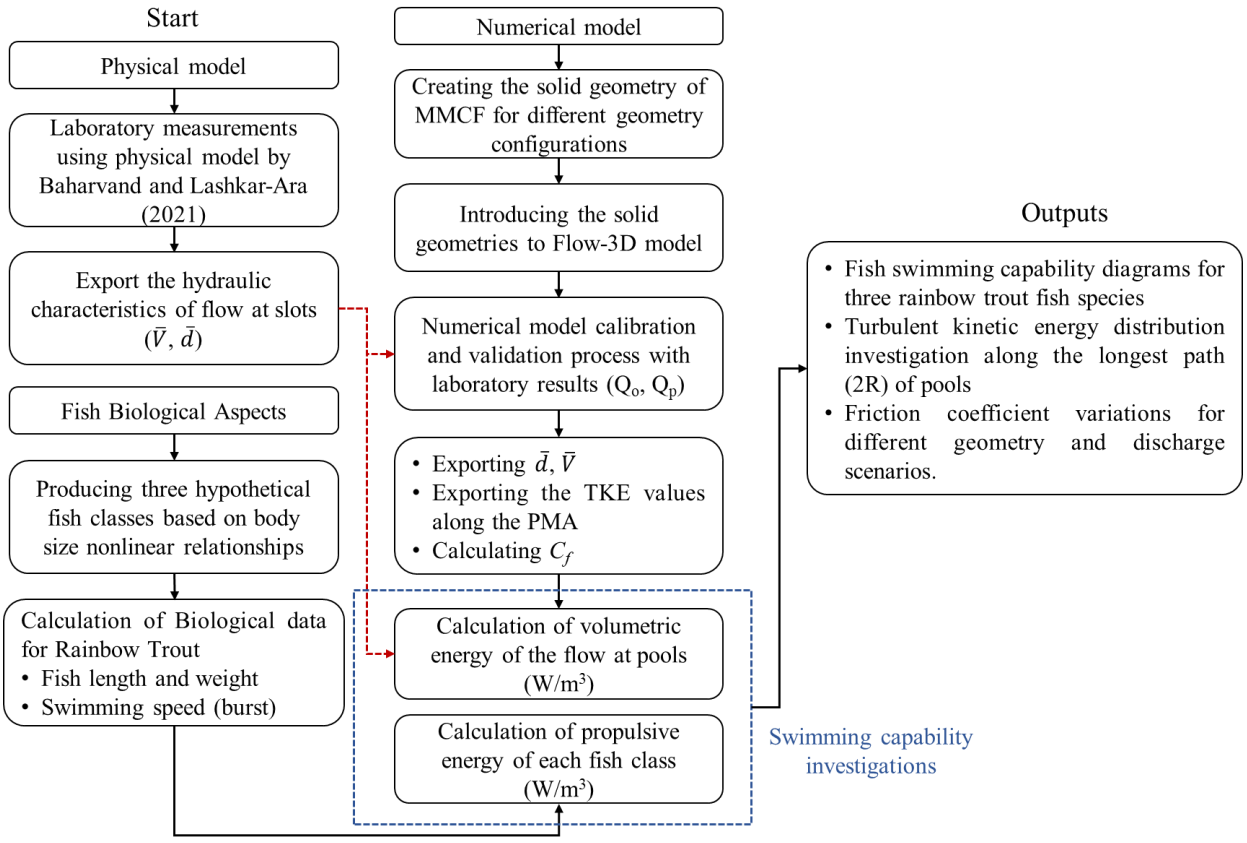

Figure 2. Framework of the present study

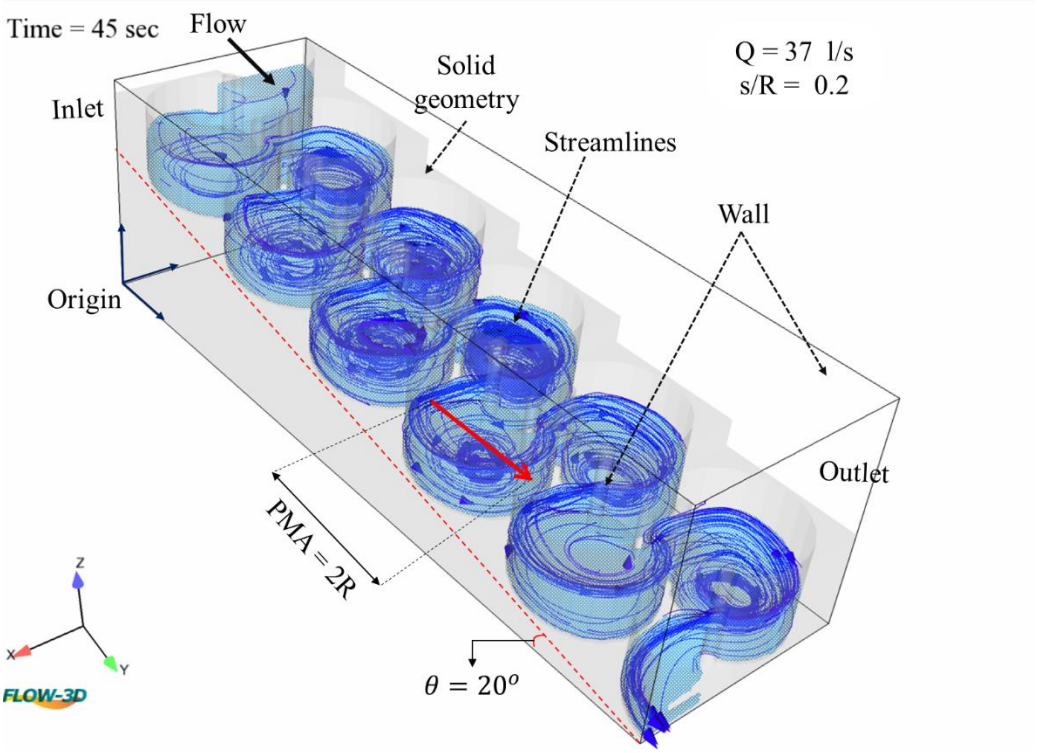

Figure 3. Three-dimensional solid geometry of MMCF and boundary condition used in CFD model

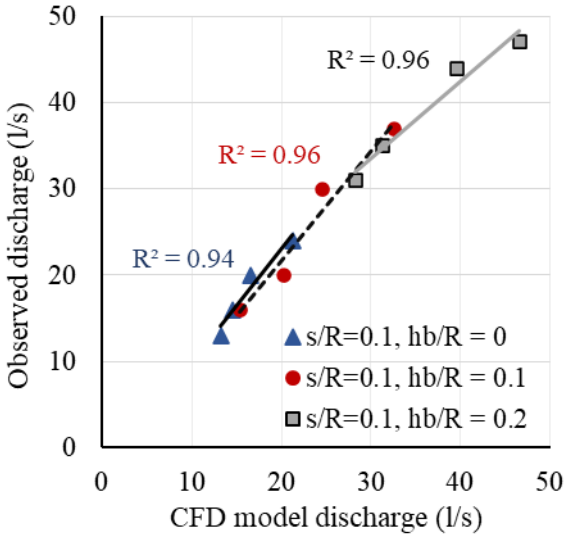

Figure 4. Physical and CFD models estimated discharge (l/s) for s/R = 0.1

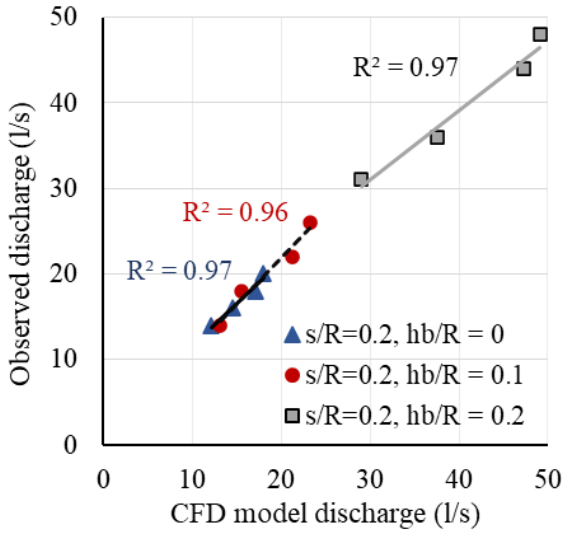

Figure 5. Physical and CFD models estimated discharge (l/s) for s/R = 0.2

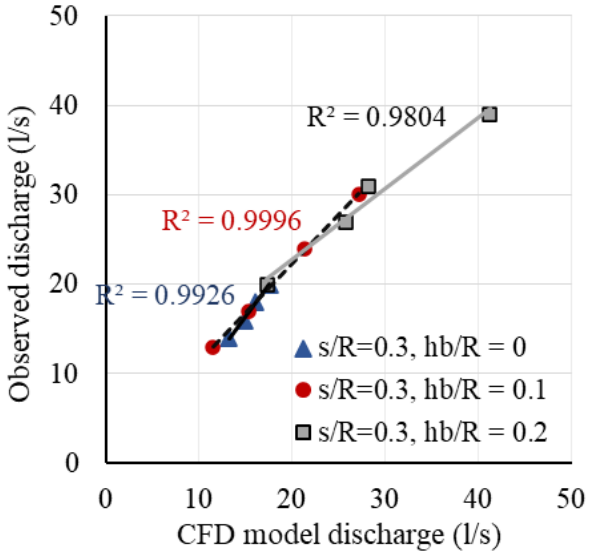

Figure 6. Physical and CFD models estimated discharge (l/s) for s/R = 0.3

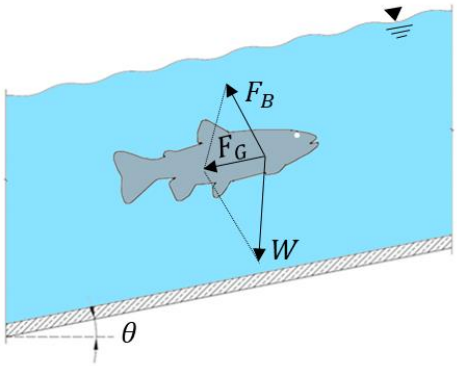

(a)

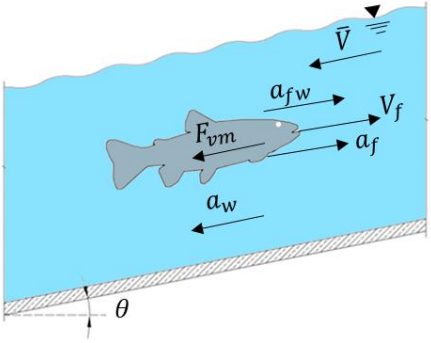

(b)

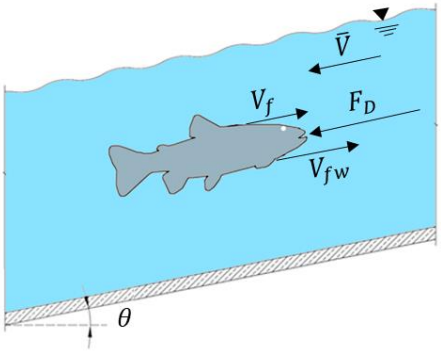

(c)

Figure 7. Forces acting on the fish body a) gravitational force b) virtual mass force c) drag force

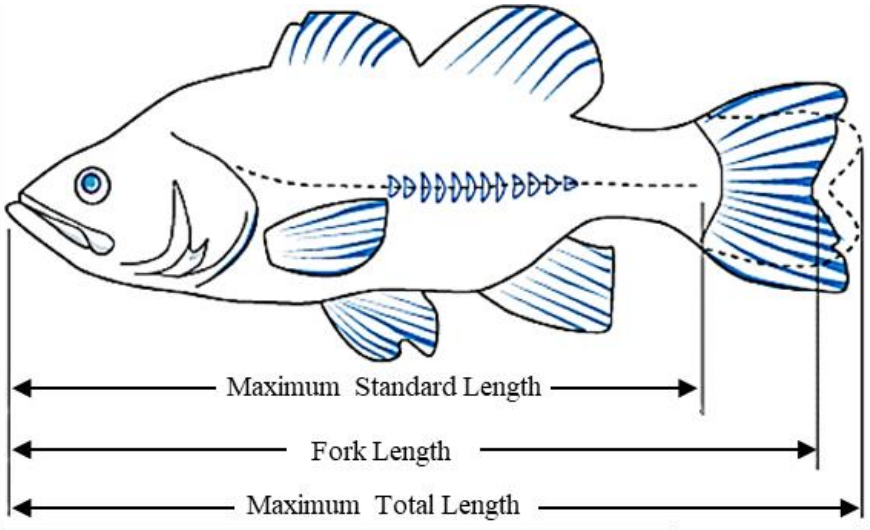

Figure 8. Different fish length measure parameters by Furniss et al. (2006)

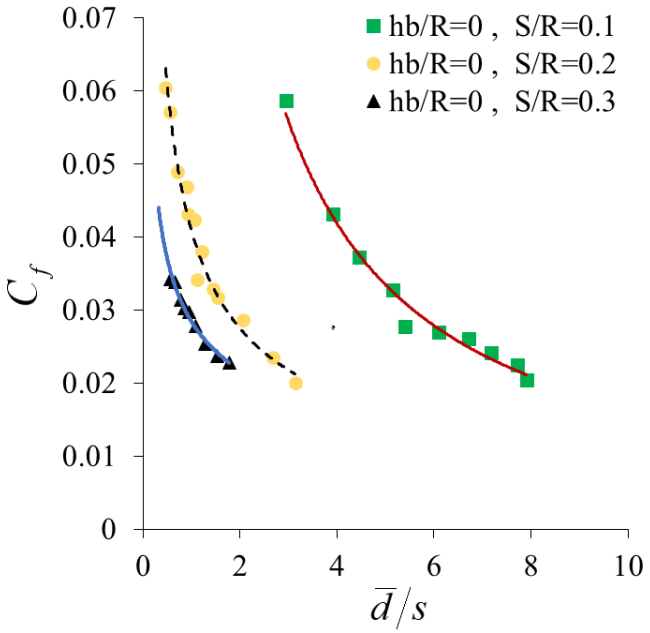

Figure 9. Fluid friction coefficient variation versus relative depth ratio (d/s) for h_b/R = 0 and s/R = 0.1,0.2, 0.3 (slope = 20%)

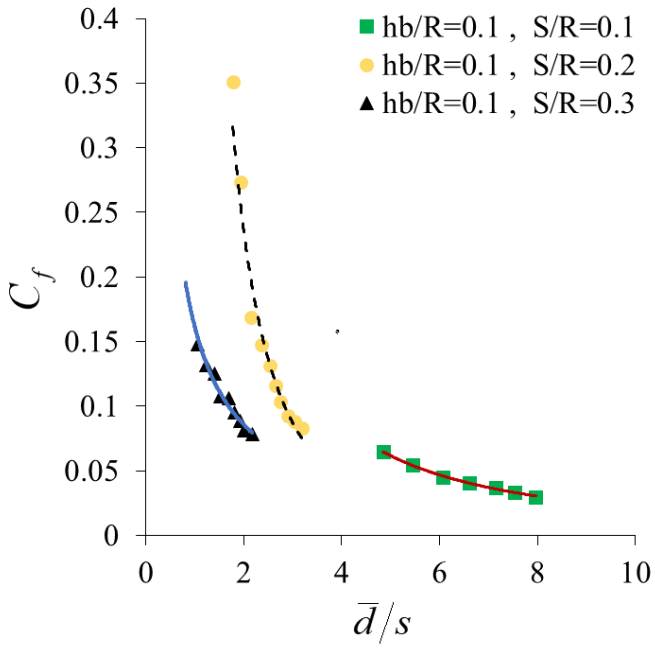

Figure 10. Fluid friction coefficient variation versus relative depth ratio (*d/s*) for hb/R = 0.1 and s/R = 0.1, 0.2,0.3 (slope = 20%)

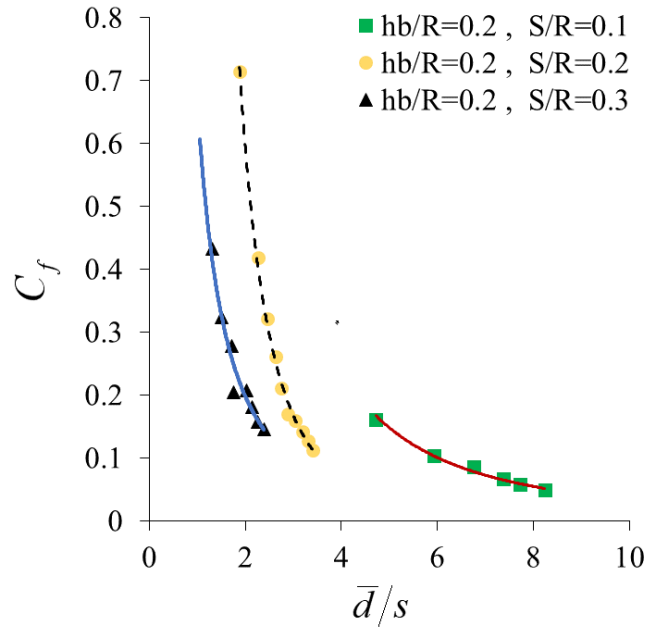

Figure 11. Fluid friction coefficient variation versus relative depth ratio (*d/s*) for h_b/R = 0.2 and s/R = 0.1, 0.2,0.3 (slope = 20%)

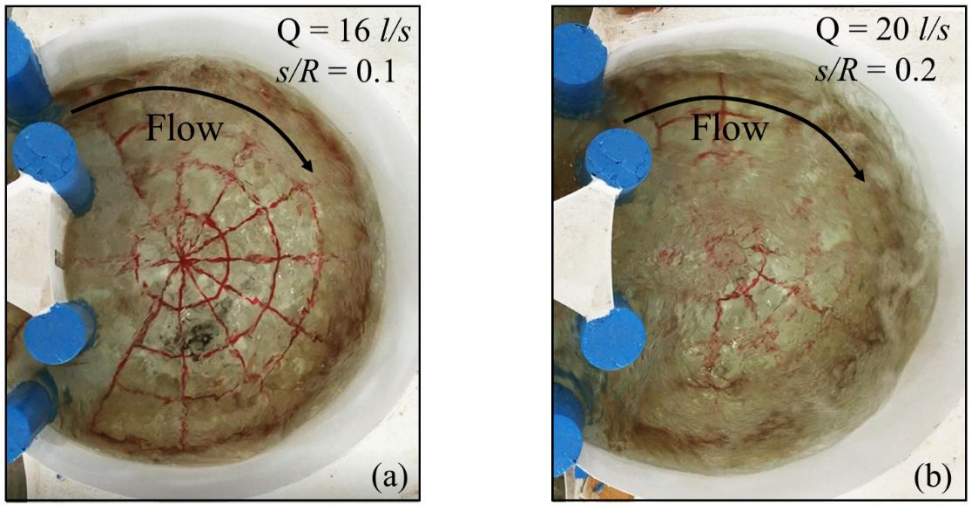

Figure 12. Qualitative assessment of flow in measuring pool no. 8 for (a) s/R = 0.1 and (b) s/R = 0.2 for d/s = 2.54

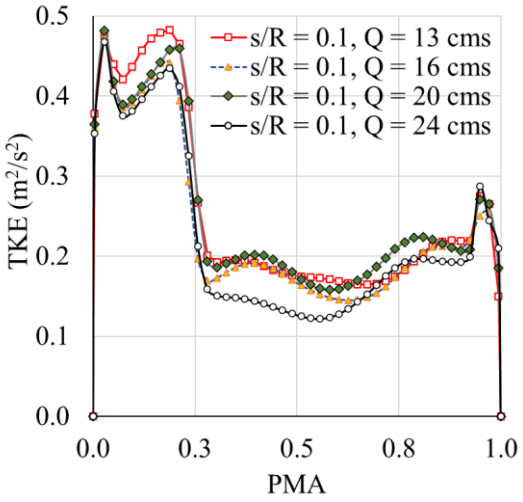

(a)

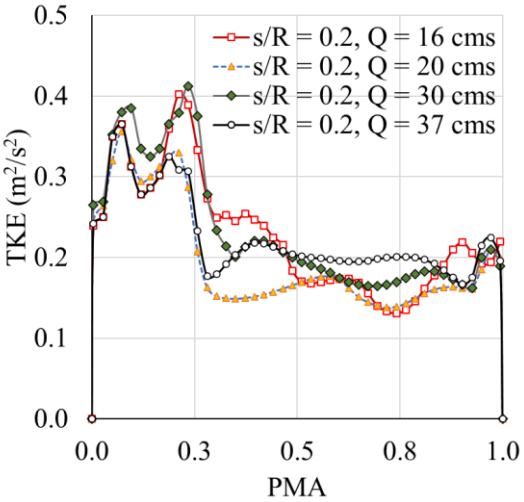

(b)

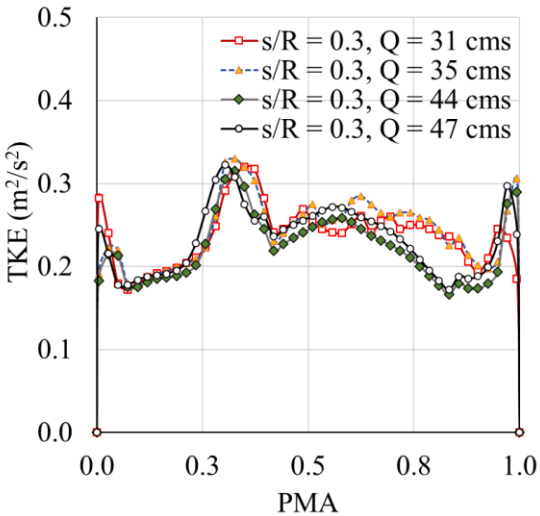

(c)

Figure 13. Turbulent Kinetic Energy (TKE) variation through PMA for h_b/R = 0 and (a) s/R = 0.1, (b) s/R = 0.2, and (c) s/R = 0.3

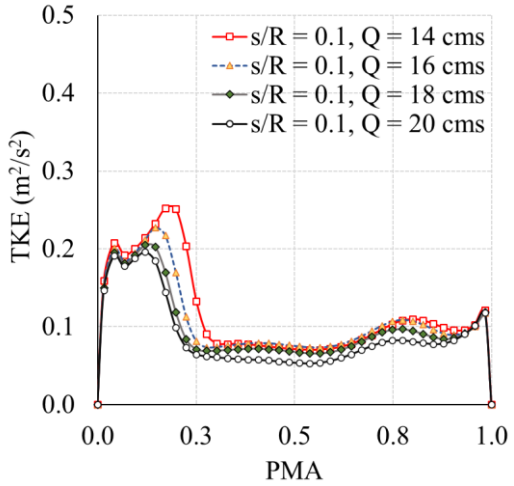

(a)

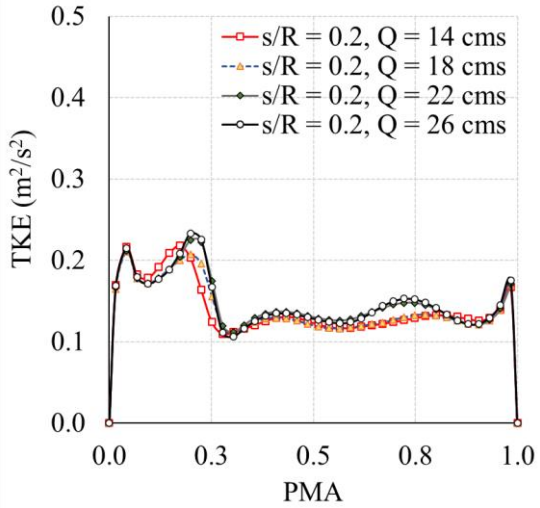

(b)

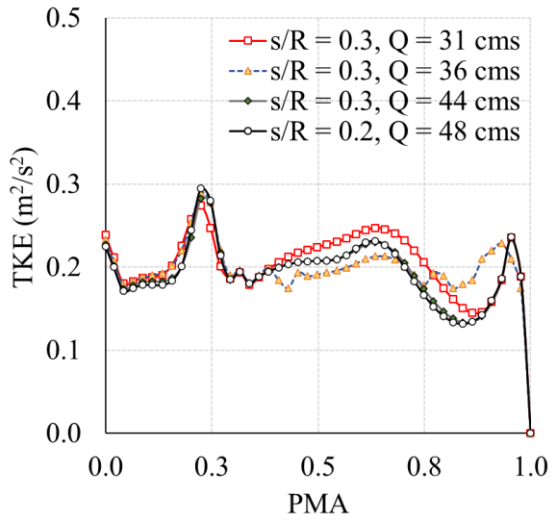

(c)

Figure 14. Turbulent Kinetic Energy (TKE) variation through PMA for h_b/R = 0.1 and (a) s/R = 0.1, (b) s/R = 0.2, and (c) s/R = 0.3

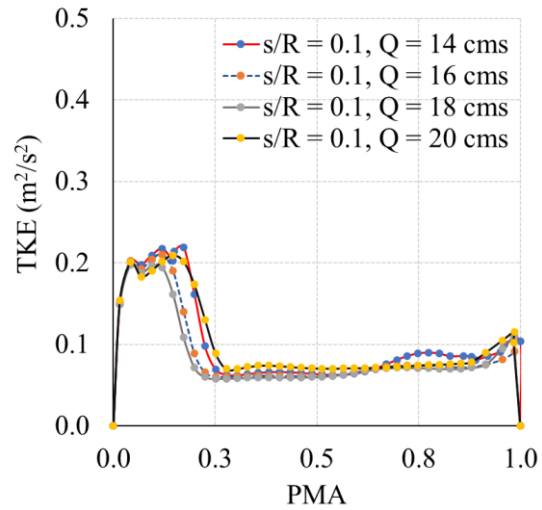

(a)

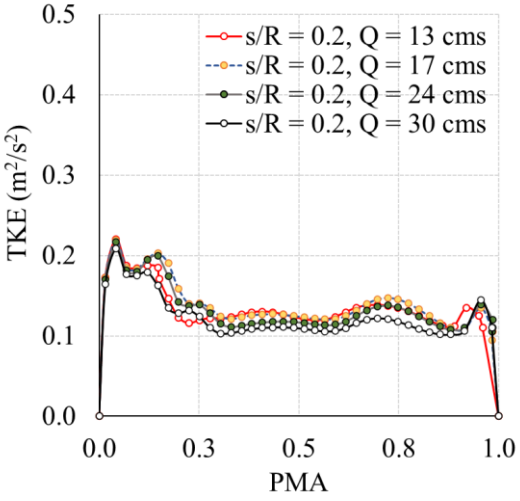

(b)

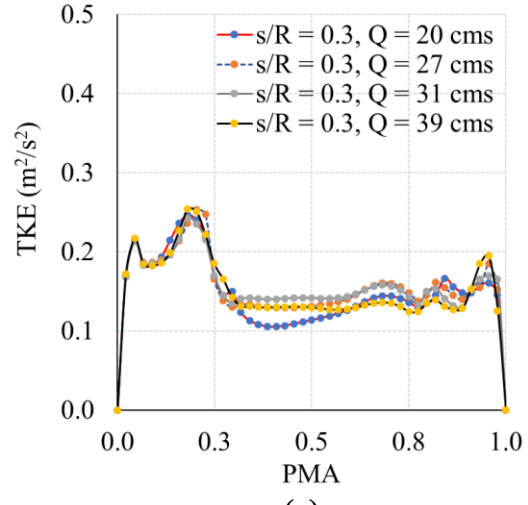

(c)

Figure 15. Turbulent Kinetic Energy (TKE) variation through PMA for h_b/R = 0.2 and (a) s/R = 0.1, (b) s/R = 0.2, and (c) s/R = 0.3

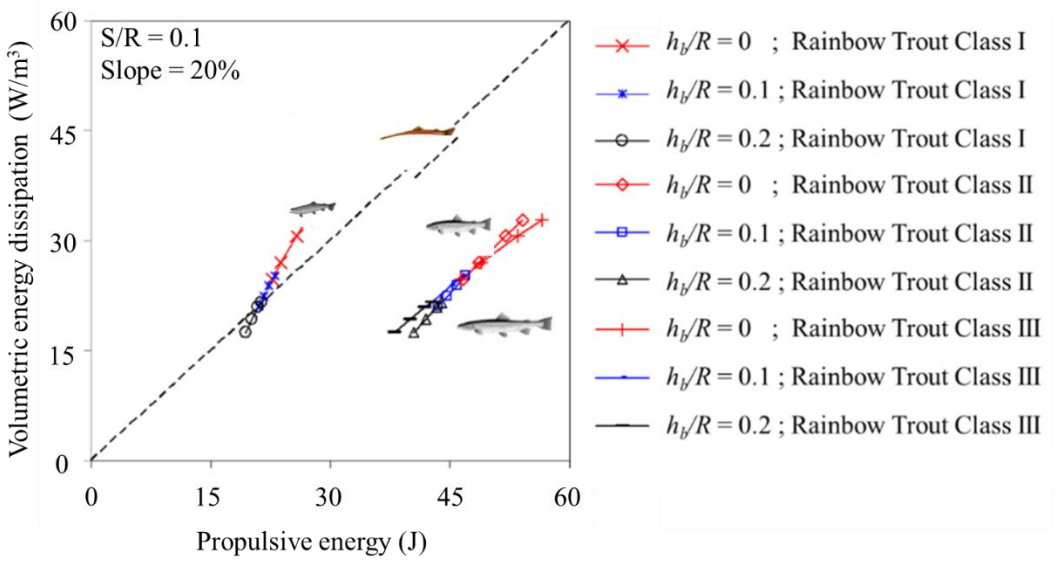

Figure 16. Potential volumetric energy (W/m^3) in MMCF pools vs. propulsive energy (J) of three rainbow trout hypothetical classes (s/R = 0.1)

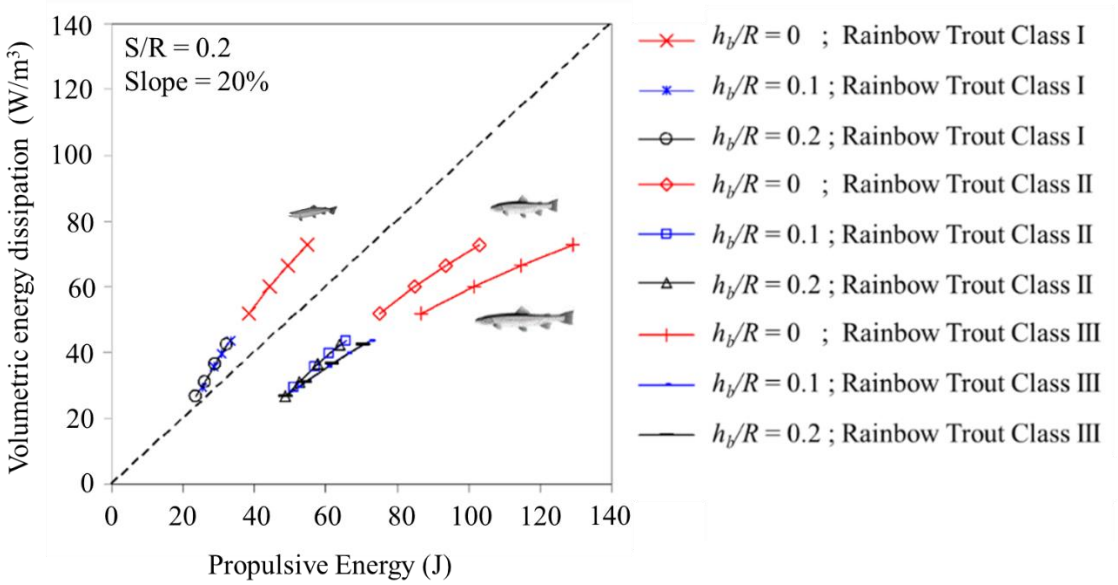

Figure 17. Potential flow volumetric energy (W/m^3) in MMCF pools vs. propulsive energy (J) of three rainbow trout hypothetical classes (s/R = 0.2)

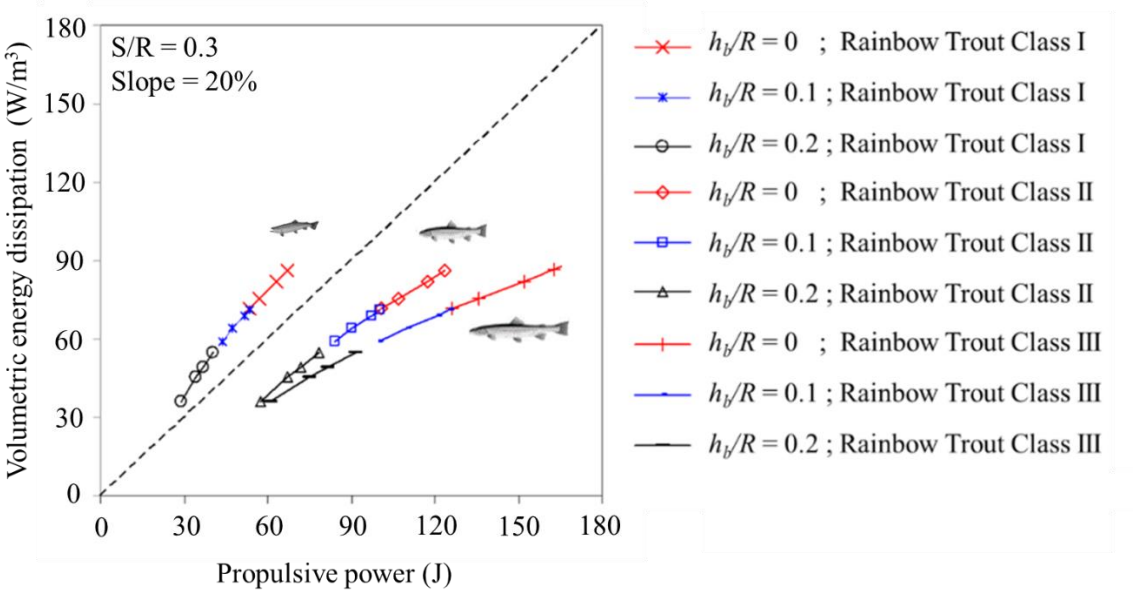

Figure 18. Potential flow volumetric energy (W/m^3) in MMCF pools vs. propulsive energy (J) of three rainbow trout hypothetical classes (s/R = 0.3)

Table 1. Discharge for each geometry scenario

s/R	h_b/R	Discharge (lit/sec)			
		Q1	Q2	Q3	Q4
0.1	0	13	16	20	24
	0.1	16	20	30	37
	0.2	31	35	44	47
0.2	0	14	16	18	20
	0.1	14	18	22	26
	0.2	31	36	44	48
0.3	0	14	16	18	20
	0.1	13	17	24	30
	0.2	20	27	31	39

Table 2. Relationships of the forces acting on fishes' body

Equation	No	Description
$F_G = WS_0$	(13)	W: fish's weight (mass) S_0: slope g: gravitational acceleration afw: relative acceleration of the fish with respect to the surrounding water (assumed to be 1.2) b: constant depending on the individual fish (assumed to be 0.4 in the present study) k: constant value (k = 4) ρ: mass density of water ν: kinematic viscosity of the surrounding water L: total length (TL) of the fish V_{fw}: swimming speed of the fish with respect to the surrounding water
$F_{vm} = 1.2\left[\frac{W}{g}\right]a_{fw}$	(14)	
$F_D = (0.036)bk\rho\nu^2 L^{1.8} V_{fw}^{1.8}$	(15)	

Table 3. Biological characteristics of synthetic rainbow trout for different body length scenarios

Fish species	Length class	TL (cm)	Burst swimming coefficients			Estimated Burst swimming speed (m/s)
			α	β	ζ	
Rainbow Trout	**Class I**	10.3	7.16	0.77	-0.46	0.313
	Class II	18.3				0.488
	Class III	28				0.677

Biography

Saman Baharvand is currently employed as a Postdoctoral Research Associate at the University of Texas at Arlington, Texas, USA, and Water Resources Research Engineer at DE Corporation (DEC), Fort Worth, Texas. He holds a Ph.D. in Civil Engineering with a specialization in Water Resources from the University of Texas at Arlington, Texas, USA, and he completed his master's degree in Water and Hydraulic Structures Engineering at Jundi-Shapur University of Technology, Iran, in 2017. Dr. Baharvand has authored or co-authored more than 25 research papers, published in various national/international journals and conference proceedings. His research interests center around physical and numerical modeling of hydro-environmental structures, sediment transport modeling, stochastic approaches, GIS development, and machine learning techniques in the area of water resources.

Babak Lashkar-Ara is an Associate Professor in the Civil Engineering Department at Jundi-Shapur University of Technology in Dezful, Iran. He earned his Ph.D. in Hydraulic Structures from Shahid Chamran University of Ahwaz, Iran, in 2009. With over 57 published research papers in well-respected international and national journals, and over 70 papers presented at Iranian national and international conferences, he is a distinguished researcher in his field. Dr. Lashkar-Ara's primary research interests are in Hydraulic Structures and River Engineering, and he continues to contribute to this field through his ongoing research efforts.